Organic Electronics 78 (2020) 105567

Contents lists available at ScienceDirect

Organic Electronics

journal homepage: http://www.elsevier.com/locate/orgel

Effect of interfacial interaction on spin polarization at organic-cobalt interface

Baoxing Liu [a], Haipeng Xie [a,*], Dongmei Niu [a,**], Shitan Wang [a], Yuan Zhao [a], Yuquan Liu [a], Lu Lyu [a,b], Yongli Gao [a,c]

[a] Hunan Key Laboratory for Super-microstructure and Ultrafast Process, College of Physics and Electronics, Central South University, Changsha, Hunan, 410012, PR China
[b] Department of Physics and Research Center OPTIMAS, University of Kaiserslautern, Erwin-Schrödinger-Straße 46, 67663, Kaiserslautern, Germany
[c] Department of Physics and Astronomy, University of Rochester, Rochester, NY, 14627, USA

ARTICLE INFO

Keywords:
Spin-resolved photoemission spectroscopy
Organic semiconductor
Cobalt
Interfacial interaction

ABSTRACT

The interface between organic semiconductors and Co thin film has been studied by spin-resolved photoemission spectroscopy. We found that the spin-polarized states of cobalt still exist when 1.0 nm rubrene or 0.7 nm C_{60} or 1.0 nm DBBA molecules deposited on Co, while 0.4 nm C8-BTBT eliminates the highly spin-polarized states of cobalt due to the desulfurization reaction occurred at the interface. The mode and strength of the interfacial interaction between organic semiconductors and magnetic electrode affect the spin-polarized states of magnetic electrode greatly. Our observations provide assistance in device design, fabrication and performance improvement in Co-based organic spintronic devices.

1. Introduction

Organic semiconductors have caused widely research interest and developed rapidly due to their strong flexibility, lightweight and good machinability [1,2]. Interfacial properties and phenomena play an important role in improving the performance of organic semiconductor devices [3,4]. Due to weak spin-orbit coupling, organic molecules are more suitable for spin transport media than inorganic substances [5]. The concept of "spinterface" was first proposed in 2010 to represent the hybrid interface between ferromagnetic and organic semiconductors [6–8]. This field is one of the hotspots in organic spintronics research and the performance of organic spin devices can be improved by obtaining well-defined contact interface [9,10]. Barraud et al. developed a spin transport model that describes the role of interfacial spin-dependent metal/molecule hybridization on the effective polarization allowing enhancement and even sign reversal of injected spins [8]. Djeghloul et al. reported a strong spin polarized interface between ferromagnetic cobalt and an amorphous carbon layer. It is shown that the highly spin-polarized organic spinterfaces at room temperature constitute a generic effect that isn't specific to a particular molecule [11]. Urbain et al. measured the prototypical system Co(001)/Cu/MnPc by spin-resolved photoemission spectroscopy. The results show that a high spin polarization of the Cu/MnPc spinterface atop ferromagnetic Co at room temperature [12]. Brambilla et al. introduced a two-dimensional oxide layer at the interface between an organic semiconductor and a ferromagnetic metal and found that the $C_{60}/Cr_4O_5/Fe$ (001) spinterface is characterized by the formation of a well-ordered fullerene layer and of strongly hybridized interface states [13]. Luque et al. investigated the adsorption of chiral organic molecules on a ferromagnetic substrate by synchrotron-radiation-based electron spectroscopies [14]. The observations show that some enantiosensitivity may appear when bonding chiral molecules to a substrate with an initial asymmetry in the population of the different spin orientations. Stöckl et al. revisit the hybrid interface formed between the prototypical molecule Alq_3 and the Co surface using spin- and angle-resolved photoemission. It is shown that the elastic scattering of the Co photoelectrons at the disordered Alq_3 overlayer leading to a redistribution of the spin-dependent spectral intensity in momentum space [15].

Rubrene (5,6,11,12-tetraphenylnaphthacene) is a π-conjugated molecular semiconductor with relatively high charge carrier mobility (~20 cm^2/V) and has potential applications as spin transport layer in spintronic systems [16]. Shim et al. reported rubrene/Co-based device have

* Corresponding author.
** Corresponding author.
E-mail addresses: xiehaipeng@csu.edu.cn (H. Xie), mayee@csu.edu.cn (D. Niu).

https://doi.org/10.1016/j.orgel.2019.105567
Received 19 April 2019; Received in revised form 13 November 2019; Accepted 15 November 2019
Available online 17 November 2019

a large room temperature tunneling magnetoresistance (TMR) of 6% and a spin-diffusion length of 13 nm in thin amorphous rubrene films [17]. 2, 7-dioctyl [1]benzothieno[3,2-b] [1]benzothiophene (C8-BTBT) is a another candidate for the organic spacer in spin valves, the mobility of C8-BTBT can record up to 43 cm^2/V during field effect transistor [18], and it also has been widely applied in various devices [19–21]. Co is most commonly used as one of the ferromagnetic electrodes for injection or detection spin-polarized current [22–25]. Most of spin diffusion lengths are determined by the electron current in related spintronic devices, direct method to detect the electron spin of these systems is particularly important, which will help to understand the working mechanism.

In this study, using Co as ferromagnetic electrode material and rubrene, C_{60}, 10,10′-dibromo-9,9′-bianthracene (DBBA), and C8-BTBT molecules as representative organic material, we directly measured the spin polarization of rubrene, C_{60}, DBBA, and C8-BTBT film covered cobalt using spin resolved photoemission spectroscopy and observed the sharp difference of the effects of the four organic films on the spin polarization of cobalt. The spin-polarized states still exist after deposition of 1.0 nm rubrene, 0.7 nm C_{60} or 1.0 nm DBBA molecules, and desulfurization reaction occurred at the C8-BTBT/Co interface removes the highly spin-polarized states of cobalt. These investigations provide assistance in performance improvements in Co-based organic spintronic devices.

2. Material and methods

The preparation of the samples and the spin-resolved photoelectron spectroscopy experiments were performed *in situ* in an interconnected ultrahigh vacuum system, which consists of an analysis chamber, a molecular beam epitaxy chamber (MBE) and an organic molecular beam evaporation (OMBE) chamber. At first, the Cu (001) substrates were prepared by repeated cycles of Ar-ion bombardment and annealing at 800 K to obtain oxygen-free and carbon-free substrate. Co layer was deposited from a rod heated by electron beam bombardment in the MBE chamber and the pressure is superior to 5×10^{-11} mbar. The deposition rate is controlled at 0.05 nm/min and the final layer thickness of the Co film was 3 nm. The Co film quality was verified by X-ray photoemission spectroscopy (XPS) and Low Energy Electron Diffraction (LEED). Organic molecules were deposited on the freshly prepared Co film in the OMBE chamber at pressure of $\sim 5 \times 10^{-9}$ mbar. All depositions were monitored with quartz crystal microbalance. The deposited organic molecules were rubrene, C_{60}, DBBA, and C8-BTBT respectively, and the thickness of the monolayer organic molecules was 0.5 nm for rubrene [26,27], 0.7 nm for C_{60} [28], 1.0 nm for DBBA [29] and 0.8 nm for C8-BTBT [30]. Then, the samples were transferred to the analysis chamber. Analysis chamber contains a variety of characterization equipment and a magnetizer coil, details please refer to our previous works [31–33]. The angle between the incident photon and the emitted photoelectron direction was 45° for spin resolved ultraviolet photoemission spectroscopy (SRUPS) and XPS. The UV light spot is about 1 mm in diameter [34].

The spin-resolved photoelectron spectroscopy was measured by Mott detector [35]. The effective Sherman factor S_{eff} of the Mott detector is 0.12. Samples have to be magnetized twice with two opposite directions to eliminate experimental asymmetry. The spin polarization component P was calculated on the basis of raw data for "left" and "right" spin channels using the following formula:

$$P = \frac{1}{S_{eff}} \frac{\sqrt{I_L^+ I_R^-} - \sqrt{I_R^+ I_L^-}}{\sqrt{I_L^+ I_R^-} + \sqrt{I_R^+ I_L^-}} \quad (1)$$

Here, I_L and I_R are two sets of intensities of "left" and "right" channels measured for "+" and "-" magnetization directions. The corresponding intensities for spin-up and spin-down channels are calculated by using

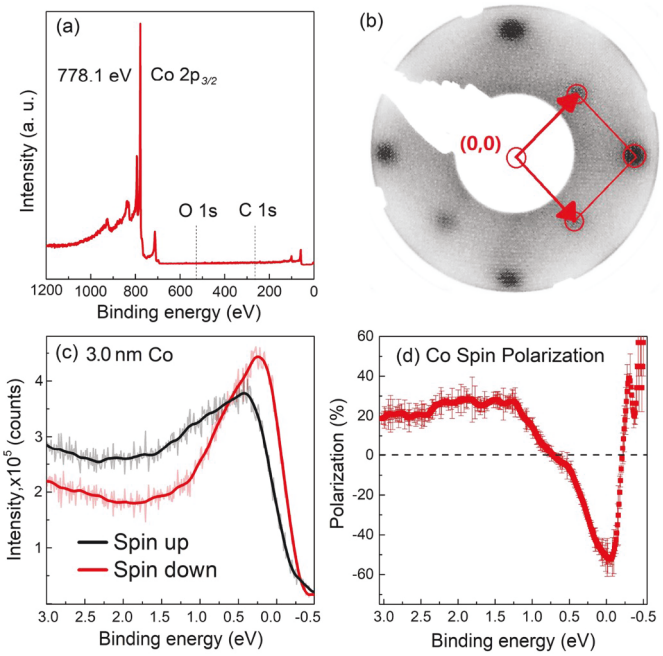

Fig. 1. (a) XPS spectra of 3 nm Co/Cu. (b) LEED image of Co (001), the diffraction spot (0, 0) and the unit cell of the $(\sqrt{2} \times \sqrt{2})$ structure is marked. (c) Spin-polarized photoemission spectra of Co (001). Black lines: spin-up, red lines: spin down, original curve is shown in translucent color. (d) In-plane spin polarization as a function of binding energy measured for uncovered Co. (For interpretation of the references to color in this figure legend, the reader is referred to the Web version of this article.)

$$I_\uparrow = I_0(1+P), I_\downarrow = I_0(1-P) \quad (2)$$

where I_0 is the total intensity of all spin channels.

3. Results and discussion

High quality thin Co films were prepared, as reflected by the clean XPS spectra, spin resolved UPS (SRUPS) and the clear LEED pattern shown in Fig. 1. The XPS full scan spectra in Fig. 1. (a) only consists of pure Co 2p and other cobalt peaks, indicating that the cobalt film is free of carbon, oxidation, and other impurity. The LEED pattern of the Cu (001) substrate is 1×1 and that of evaporated cobalt film is reconstructed Cu (001)$-(\sqrt{2} \times \sqrt{2})R45° -$ Co [36,37]. As shown in Fig. 1(b), a clear LEED pattern of face-centered cubic (fcc) Co, the diffraction spot (0, 0) is sketched in panel and the reciprocal unit cell of the $(\sqrt{2} \times \sqrt{2})$ structure is marked by a red rhombus, indicating high crystalline quality. The Co/Cu(001) system has been extensively investigated in the past, the easy magnetization axis of 3 nm Co films lies in-plane [38–41]. Fig. 1(c) shows spin-polarized photoemission spectra of Co films. Black lines (spin-up) and red lines (spin down) represents fitting results with the polynomial function. The original curve is shown in translucent color. Fig. 1(d) shows spin polarization as a function of binding energy measured for bare Co. It can be seen from Fig. 1(c) and (d), the in-plane spin polarization of uncovered Co is strongly negative close to E_F, and the fitting result is approximately 55%, consistent with the previous research results [39].

Fig. 2 shows spin-polarized photoemission spectra and corresponding spin polarization of rubrene/Co(001) for 0.2 nm, 0.5 nm, and 1.0 nm rubrene. All measurements have the same incident photon intensity, the intensity of the spin-polarized photoemission spectra is initial data. In Fig. 2(a), (b) and (c), the spin polarization decay with increasing of rubrene thickness and the corresponding value is negative about 30%, 20% and 10% at the Fermi level, respectively. The photoemission

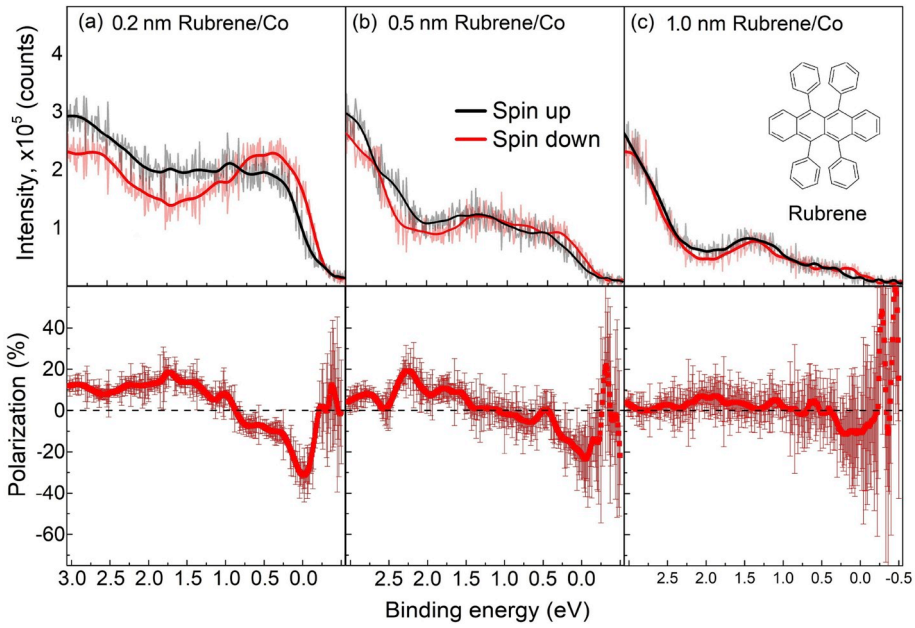

Fig. 2. Spin-polarized photoemission spectra and corresponding spin polarization of rubrene/Co(001) for 0.2 nm, 0.5 nm, and 1.0 nm rubrene thickness. The insets show the rubrene molecules.

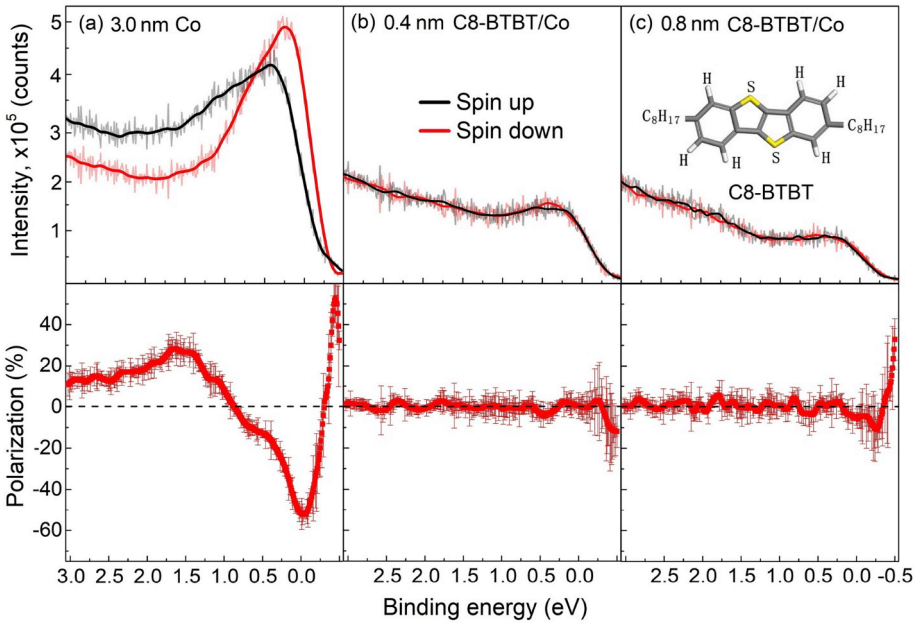

Fig. 3. Spin-polarized photoemission spectra and corresponding spin polarization of C8-BTBT/Co (001) for 0, 0.4 nm, and 0.8 nm C8-BTBT thickness. The insets show the C8-BTBT molecules.

intensity of rubrene/Co decreases slowly with increasing rubrene thickness.

In addition, we also performed spin-resolved photoemission spectroscopy measurements on C_{60}/Co and DBBA/Co interfaces (not shown, see the Supporting Information). The results are similar to that of rubrene/Co, which also displayed decreased spin polarization with the organic film thickness and after 0.7 nm C_{60} or 1 nm DBBA deposition highly spin-polarized states still exist in these interfaces.

However, spin-polarized photoemission spectra of C8-BTBT/Co (001) and its variation with film thickness is quite different from those of C_{60}, rubrene and DBBA on Co, as shown in Fig. 3. The highly spin-polarized states near the E_F for clean Co, shown in Fig. 3(a) is greatly depressed by the 0.4 nm C8-BTBT deposition. The photoemission intensity of C8-BTBT/Co decreases sharply with increasing C8-BTBT thickness in an exponential manner (see Fig. 3(b) and (c)). Very low C8-BTBT coverage strongly modifies the interfacial electronic structure and leads to the disappearance of the spin-polarized states of Co film.

To better understand the different spin-dependent properties of rubrene, C_{60} and C8-BTBT with Co interfaces, we investigated the chemical characteristics using XPS. As shown in Fig. 4, we plotted the C 1s core level peak as a function of rubrene, C_{60} and C8-BTBT coverage. In order to facilitate the interface hybridization analysis, we fit all of the C 1s spectra with three peaks. Translucent blue peak corresponds to the C 1s in cobalt carbides [42], which confirms that a small amount of C atoms binds to Co atoms at the interface. Translucent red peak and translucent green correspond to of graphite-like sp2 and C–O bonds [43,

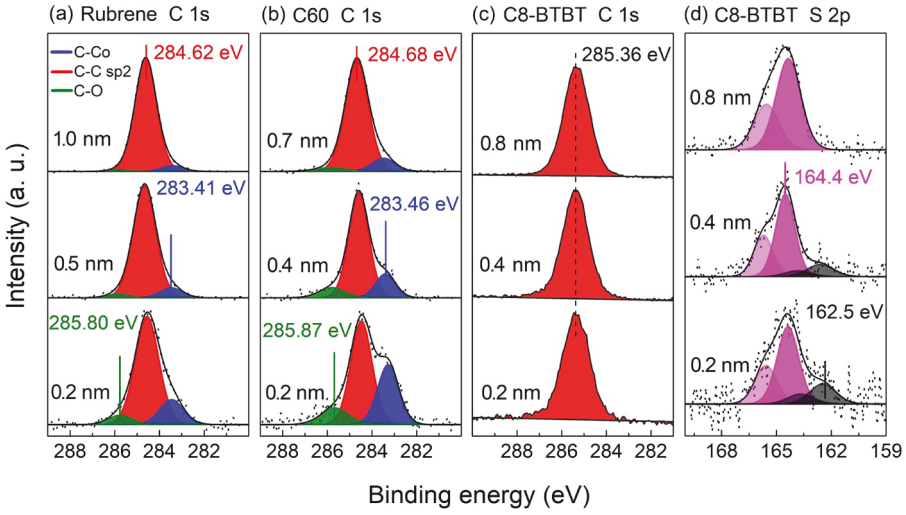

Fig. 4. Evolution of XPS spectra as a function of rubrene, C_{60} and C8-BTBT thickness deposited on Co. (a) rubrene C 1s, (b) C_{60} C 1s, (c) C8-BTBT C 1s, (d) C8-BTBT S 2p.

44]. As shown Fig. S3, we find that there is no oxygen on the Co film, and then the O 1s peak appears after C_{60} molecules deposition. Thus, the C–O bonds come from the OMBE chamber with a pressure of 5×10^{-8} mbar during organic molecular growth. In Fig. 4(a), at the initial rubrene deposition, the proportion of C–Co and C–O bonds is very small. The C 1s peak is located at ca. 284.62 eV which can be attribute to the carbon components in rubrene, agree with previous reports [45,46]. With the deposition of rubrene, the peak has barely moved, indicating that the interfacial rubrene molecules are chemically similar to that of the rubrene molecules uncontact with Co substrate except for the small C–Co component. Hou et al. reported that there is not intermixing at the rubrene/Co interface due to no significant change of the coercive force of Co film as the rubrene thickness increases on rubrene/Co(001) [47]. The unchanged main part of C1s in the present spectra support Hou's conclusion that no apparent chemical reaction takes place between Co and rubrene but for some limited charge transfer between the interfacial rubrene and the Co substrate. Raman et al. reported that similar magnetic moments for the free bottom Co layer were also observed in the parallel and antiparallel states at the rubrene/Co interface [48]. We thus inferred that the physical adsorption of rubrene may be one of the possible reason that the spin-polarized states of Co film are barely affected by rubrene deposition. Similar C1s components and variation with film thickness were also found for C_{60}/Co system, as shown in Fig. 4 (b), C–Co peaks are located at 283.46 eV and C–O peaks are located at 285.87 eV at the initial C_{60} deposition. These two bonds exist mainly at the interface and gradually attenuated as the C_{60} thickness increases. The 0.7 nm spectrum consists mainly of C–C sp2 bonds. The case of DBBA (Fig. S4) is similar to that of C_{60}. The reduced spin polarization at the Fermi level as the increasing rubrene, C_{60}, and DBBA thickness can be attribute to the interface hybridization forms C–Co. Furthermore, we compared the change of the spin polarization as the increasing of the thickness. At the initial deposition, the spin polarization is about 30%, 30%, and 50% respectively for Co film covered by Rubrene, DBBA, C_{60} molecule. It is find that the spin polarization of Co film covered by Rubrene and DBBA molecule decreases faster than that of C_{60} molecule. The trend of change was the same as the increasing of the organic molecules thickness. By comparison with the structures of the Rubrene, DBBA, C_{60} molecule, it is find that the C_{60} is a spherical structure and the Rubrene and DBBA are aspherical structure. So, we assume that this phenomenon is due to the difference of the structure of organic molecules.

The C 1s component of C8-BTBT at the interface layer is quite different from those of rubrene, C_{60} and DBBA, as shown in Fig. 4(c). Although the C atoms in C8-BTBT is bond in a similar conjugated way as in that of rubrene, the C–Co component are not observable which indicates that the charge transfer, if there is any, is not between the Co substrate and C atoms. So, we examined the S 2p peaks and found an S–Co component in the interfacial C8-BTBT, which means the charge transfer or bonding across the interface take place mainly between sulfur atom and Co substrate. In Supporting Information Fig. S5(b), evolution of Co 2p spectra as a function of C8-BTBT thickness deposited on Co. With the increase of thickness, the Co 2p core levels shifts toward higher binding energy. It is helpful to compare the energy differences of S–Co, C–Co peaks with their main peaks. The S–Co peak locates at 162.5 eV, 1.9 eV above that of main peak of 164.4 eV, while the C–Co peak locates 1.2 eV above the main C 1s peak of 284.6 eV. The much larger S–Co energy difference indicate more charge transfer from Co substrate to the S atoms which means a much stronger interaction and tight bond occur between the Co film and C8-BTBT over layer. Strong interaction may result in great changes in the valence band structures and even the chemical components changes. We examined the S:C ratio for 0.4 nm C8-BTBT film and found S: C is 1:13, larger than the stoichiometric 1:15, consistent with previous research of C8-BTBT/Co surface analysis [49, 50]. The strong interaction between Co and S break down the C–S bonding and results in strong S–Co bonding and desulfurization of C8-BTBT. The desulfurization disrupts the thiophene rings in C8-BTBT and the chemical products of volatile hydrocarbons leaves the surface, resulting in an increase of the relative abundance of sulfur in the interface region. The charge transfer from cobalt to sulfur and the tight bonding of surfur atoms on the surface is probably the main reason for the sharp decrease of the spin polarization at the C8-BTBT/Co interface. Whether removes the spin-polarized states of cobalt is only related to S or only specific to C8-BTBT. Since spin-polarization tunneling current can transport through the S layer at Sulfur-covered Fe/W(110) system [51], it is shown that removes the spin-polarized states of cobalt should only be related to specific molecules such as C8-BTBT.

Comparing the spin polarization of Co layer covered by different organic layer (rubrene, C_{60}, DBBA and C8-BTBT), we found that the reduced spin polarization at the Fermi level as the increasing rubrene, C_{60} and DBBA thickness can be attribute to the interface hybridization of C–Co bonds. As the increasing of organic molecules thickness, the interface hybridization increases due to more organic molecules interaction with Co, which would lead to decay of the spin polarization. The C8-BTBT molecular film leads to the disappearance of the spin-polarized states of Co, implying that chemical reaction between cobalt and thiophene rings has greatly depressed the correlations of cobalt electrons

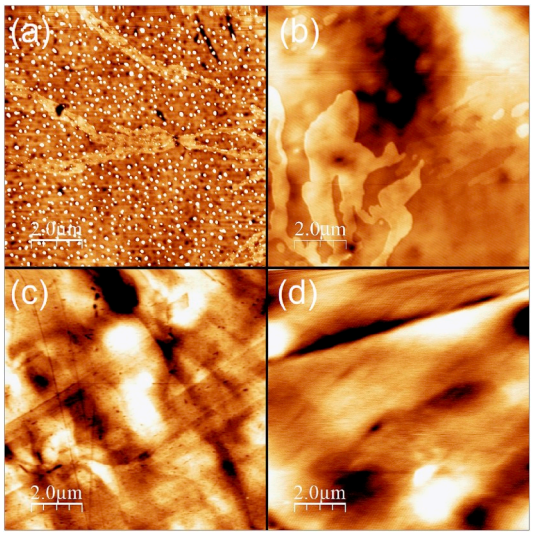

Fig. 5. The AFM topography image (10 μm × 10 μm) of (a) 1.0 nm Rubrene, (b) 0.8 nm C8-BTBT, (c) 1.0 nm DBBA, (d) 0.7 nm C_{60} deposited on Co(001).

and the spin polarization.

Furthermore, we check the crystal structure and surface morphology of organic molecules deposition on Co film by using LEED and atomic force microscope (AFM). As shown in Fig. S6∼S9, we find that the LEED pattern disappear at the initial organic molecules deposition and there is no new LEED pattern appear as the increasing of organic molecules thickness. It is indicated that the organic molecules does not crystallize. Meanwhile, The AFM measurement shows that the surface morphologies on the Co film is different for different organic molecules. The growth mode of Rubrene deposition on Co film is Volmer-Weber and there is isolated island when the Rubrene thickness reaches 1.0 nm, as shown in Fig. 5(a). The 0.8 nm C8-BTBT is partial coverage on Co film (Fig. 5(b)) and 1.0 nm DBBA is almost completely coverage (Fig. 5(c)). For 0.7 nm C_{60} (Fig. 5(d)), it is almost invisible from the AFM topography image and the possible reason is that the C_{60} desorption occurs in ambient air. We find that the Rubrene and DBBA show a different surface topography, but they have a same decay trend of the spin polarization. Meanwhile, the topography of DBBA and C8-BTBT on Co film is similar to each other, but they show an entirely different decay of the spin polarization. Combined with the result of upper experiment, we suspect that the interface interaction between Co and organic molecules is dominated on the decay of the spin polarization.

4. Conclusions

In conclusion, the spin polarization of rubrene, C_{60}, DBBA, and C8-BTBT film covered cobalt were studied by SRUPS. The results show that the reduced spin polarization of Co film when the rubrene, C_{60}, or DBBA deposited on Co film, which can be attributed to the interface hybridization forms of C–Co bonds. Very low C8-BTBT coverage (<0.4 nm) strongly depress the spin polarization of Co film due to the desulfurization reaction occurred at the C8-BTBT/Co interface. Weak hybridization can modify and depress the polarization gradually within a subnanometer, while desulfurization reaction can eliminate the polarization by a low organic film coverage <0.4 nm. Our research is helpful for the design, fabrication and performance improvement of Co-based organic spintronic devices.

Supplementary Material

See supplementary material for the spin-polarized photoemission spectra of C_{60}/Co(001) and DBBA/Co(001), O 1s spectra of C_{60} deposited on Co, C 1s spectra of DBBA deposited on Co, Co 2p spectra of rubrene and C8-BTBT deposited on Co, LEED and AFM image of Rubrene, C8-BTBT, C60, and DBBA deposited on Co (001).

Declaration of competing interest

The authors declared that they have no conflicts of interest to this work. We declare that we do not have any commercial or associative interest that represents a conflict of interest in connection with the work submitted.

Acknowledgments

We thank the financial support by the National Key Research and Development Program of China (Grant Nos. 2017YFA0206602) and the National Natural Science Foundation of China (Grant Nos. 11334014 and 51802355). H.X. acknowledges the support by the Natural Science Foundation of Hunan Province (Grant No. 2018JJ3625). Y.G. acknowledges the support by the National Science Foundation (Grant Nos. DMR-1303742 and CBET-1437656).

Appendix A. Supplementary data

Supplementary data to this article can be found online at https://doi.org/10.1016/j.orgel.2019.105567.

References

[1] N. Koch, Organic electronic devices and their functional interfaces, ChemPhysChem 8 (2007) 1438–1455.
[2] Y.L. Gao, Surface analytical studies of interfaces in organic semiconductor devices, Math. Sci. Eng. R. 68 (2010) 39–87.
[3] H. Ishii, K. Sugiyama, E. Ito, K. Seki, Energy level alignment and interfacial electronic structures at organic/metal and organic/organic interfaces, Adv. Mater. 11 (1999) 605–625.
[4] A. Kahn, N. Koch, W. Gao, Electronic structure and electrical properties of interfaces between metals and π-conjugated molecular films, J. Polym. Sci., Part B: Polym. Phys. 41 (2003) 2529–2548.
[5] D.S. McClure, Spin-orbit interaction in aromatic molecules, J. Chem. Phys. 20 (1952) 682–686.
[6] J. Brede, N. Atodiresei, S. Kuck, P. Lazic, V. Caciuc, Y. Morikawa, G. Hoffmann, S. Blugel, R. Wiesendanger, Spin- and energy-dependent tunneling through a single molecule with intramolecular spatial resolution, Phys. Rev. Lett. 105 (2010), 047204.
[7] N. Atodiresei, J. Brede, P. Lazic, V. Caciuc, G. Hoffmann, R. Wiesendanger, S. Blugel, Design of the local spin polarization at the organic-ferromagnetic interface, Phys. Rev. Lett. 105 (2010), 066601.
[8] C. Barraud, P. Seneor, R. Mattana, S. Fusil, K. Bouzehouane, C. Deranlot, P. Graziosi, L. Hueso, I. Bergenti, V. Dediu, F. Petroff, A. Fert, Unravelling the role of the interface for spin injection into organic semiconductors, Nat. Phys. 6 (2010) 615–620.
[9] F. Borgatti, I. Bergenti, F. Bona, V. Dediu, A. Fondacaro, S. Huotari, G. Monaco, D. A. MacLaren, J.N. Chapman, G. Panaccione, Understanding the role of tunneling barriers in organic spin valves by hard x-ray photoelectron spectroscopy, Appl. Phys. Lett. 96 (2010) 12.
[10] I. Bergenti, A. Riminucci, E. Arisi, M. Murgia, M. Cavallini, M. Solzi, F. Casoli, V. Dediu, Magnetic properties of Cobalt thin films deposited on soft organic layers, J. Magn. Magn. Mater. 316 (2007) E987–E989.
[11] F. Djeghloul, G. Garreau, M. Gruber, L. Joly, S. Boukari, J. Arabski, H. Bulou, F. Scheurer, A. Hallal, F. Bertran, P. Le Fèvre, A. Taleb-Ibrahimi, W. Wulfhekel, E. Beaurepaire, S. Hajjar-Garreau, P. Wetzel, M. Bowen, W. Weber, Highly spin-polarized carbon-based spinterfaces, Carbon 87 (2015) 269–274.
[12] E. Urbain, F. Ibrahim, M. Studniarek, F. Ngassam, L. Joly, J. Arabski, F. Scheurer, F. Bertran, P.L. Fèvre, G. Garreau, Cu metal/Mn phthalocyanine organic spinterfaces atop Co with high spin polarization at room temperature, Adv. Funct. Mater. 28 (2018), 1707123.
[13] A. Brambilla, A. Picone, S. Achilli, G. Fratesi, A. Lodesani, A. Calloni, G. Bussetti, M. Zani, M. Finazzi, L. Duò, F. Ciccacci, Effects of the introduction of a chromium oxide monolayer at the C60/Fe(001) interface, J. Appl. Phys. 125 (2019), 142907.
[14] F.J. Luque, M.A. Nino, M.J. Spilsbury, I.A. Kowalik, D. Arvanitis, J.J. de Miguel, Enantiosensitive bonding of chiral molecules on a magnetic substrate investigated by means of electron spectroscopies, Chimia 72 (2018) 418–423.
[15] J. Stöckl, A. Jurenkow, N. Großmann, M. Cinchetti, B. Stadtmüller, M. Aeschlimann, Spin- and angle-resolved photoemission study of the Alq3/Co interface, J. Phys. Chem. C 122 (2018) 6585–6592.
[16] V. Podzorov, E. Menard, A. Borissov, V. Kiryukhin, J.A. Rogers, M.E. Gershenson, Intrinsic charge transport on the surface of organic semiconductors, Phys. Rev. Lett. 93 (2004), 086602.

[17] J.H. Shim, K.V. Raman, Y.J. Park, T.S. Santos, G.X. Miao, B. Satpati, J.S. Moodera, Large spin diffusion length in an amorphous organic semiconductor, Phys. Rev. Lett. 100 (2008), 226603.
[18] Y. Yuan, G. Giri, A.L. Ayzner, A.P. Zoombelt, S.C. Mannsfeld, J. Chen, D. Nordlund, M.F. Toney, J. Huang, Z. Bao, Ultra-high mobility transparent organic thin film transistors grown by an off-centre spin-coating method, Nat. Commun. 5 (2014) 3005.
[19] C.N. Warwick, D. Venkateshvaran, H. Sirringhaus, Accurate on-chip measurement of the Seebeck coefficient of high mobility small molecule organic semiconductors, Apl. Mater. 3 (2015), 096104.
[20] Y.L. Huang, J. Sun, J.D. Zhang, S.T. Wang, H. Huang, J. Zhang, D.H. Yan, Y.L. Gao, J.L. Yang, Controllable thin-film morphology and structure for 2,7-dioctyl[1]benzothieno[3,2-b][1]benzothiophene (C8BTBT) based organic field-effect transistors, Org. Electron. 36 (2016) 73–81.
[21] Y. Zhao, X.L. Liu, L. Lyu, L. Li, W.J. Tan, S.T. Wang, C. Wang, D.M. Niu, H.P. Xie, H. Huang, Fullerene (C 60) interlayer modification on the electronic structure and the film growth of 2, 7-diocty [1] benzothieno-[3, 2-b] benzothiophene on SiO 2, Synthetic, Met 229 (2017) 1–6.
[22] M. Cinchetti, K. Heimer, J.P. Wustenberg, O. Andreyev, M. Bauer, S. Lach, C. Ziegler, Y. Gao, M. Aeschlimann, Determination of spin injection and transport in a ferromagnet/organic semiconductor heterojunction by two-photon photoemission, Nat. Mater. 8 (2009) 115–119.
[23] O. Andreyev, Y.M. Koroteev, M.S. Albaneda, M. Cinchetti, G. Bihlmayer, E. Chulkov, J. Lange, F. Steeb, M. Bauer, P. Echenique, Spin-resolved two-photon photoemission study of the surface resonance state on Co/ Cu (001), Phys. Rev. B 74 (2006), 195416.
[24] R. Lin, F. Wang, J. Rybicki, M. Wohlgenannt, K.A. Hutchinson, Distinguishing between tunneling and injection regimes of ferromagnet/organic semiconductor/ferromagnet junctions, Phys. Rev. B 81 (2010), 195214.
[25] Z.H. Xiong, D. Wu, Z.V. Vardeny, J. Shi, Giant magnetoresistance in organic spin-valves, Nature 427 (2004) 821–824.
[26] M.C. Blüm, W.D. Schneider, Supramolecular Assembly, Chirality, and Electronic Properties of Rubrene Studied by STM and STS, EPFL, Lausanne.
[27] B.A. Kowert, N.C. Dang, K.T. Sobush, L.G. Seele, Diffusion of aromatic hydrocarbons inn-alkanes and cyclohexanes, J. Phys. Chem. A 105 (2001) 1232–1237.
[28] J.E. Fischer, P.A. Heiney, A.R. McGhie, W.J. Romanow, A.M. Denenstein, J. P. McCauley Jr., A.B. Smith 3rd, Compressibility of solid c60, Science 252 (1991) 1288–1290.
[29] G. Tian, Y.X. Shen, B.C. He, Z.Q. Yu, F. Song, Y.H. Lu, P.S. Wang, Y.L. Gao, H. Huang, Effects of monolayer Bi on the self-assembly of DBBA on Au(111), Surf. Sci. 665 (2017) 89–95.
[30] H. Kobayashi, N. Kobayashi, S. Hosoi, N. Koshitani, D. Murakami, R. Shirasawa, Y. Kudo, D. Hobara, Y. Tokita, M. Itabashi, Hopping and band mobilities of pentacene, rubrene, and 2,7-dioctyl[1]benzothieno[3,2-b][1]benzothiophene (C8-BTBT) from first principle calculations, J. Chem. Phys. 139 (2013), 014707.
[31] H.P. Xie, D.M. Niu, L. Lyu, H. Zhang, Y.H. Zhang, P. Liu, P. Wang, D. Wu, Y.L. Gao, Evolution of the electronic structure of C60/La0. 67Sr0. 33MnO3 interface, Appl. Phys. Lett. 108 (2016), 011603.
[32] H.P. Xie, H. Huang, N.T. Cao, C.H. Zhou, D.M. Niu, Y.L. Gao, Effects of annealing on structure and composition of LSMO thin films, Phys. B Condens. Matter 477 (2015) 14–19.
[33] X.L. Liu, C.G. Wang, C.C. Wang, I.F. Irfan, Y.L. Gao, Interfacial electronic structures of buffer-modified pentacene/C-60-based charge generation layer, Org. Electron. 17 (2015) 325–333.
[34] B.X. Liu, H.P. Xie, D.M. Niu, H. Huang, C. Wang, S.T. Wang, Y. Zhao, Y.Q. Liu, Y. L. Gao, Interface electronic structure between Au and black phosphorus, J. Phys. Chem. C 122 (2018) 18405–18411.
[35] J. Kessler, Polarized Electrons, Springer, Berlin, 1985.
[36] E. Navas, P. Schuster, C.M. Schneider, J. Kirschner, A. Cebollada, C. Ocal, R. Miranda, J. Cerdá, P. de Andrés, Crystallography of epitaxial face centered tetragonal Co/Cu (100) by low energy electron diffraction, J. Magn. Magn. Mater. 121 (1993) 65–68.
[37] L. Gonzalez, R. Miranda, M. Salmerón, J.A. Vergés, F. Ynduráin, Experimental and theoretical study of Co adsorbed at the surface of Cu: reconstructions, charge-density waves, surface magnetism, and oxygen adsorption, Phys. Rev. B 24 (1981) 3245.
[38] A. Clarke, G. Jennings, R.F. Willis, P.J. Rous, J.B. Pendry, A LEED determination of the structure of cobalt overlayers grown on a single-crystal Cu (001) substrate, Surf. Sci. 187 (1987) 327–338.
[39] P. Krams, F. Lauks, R.L. Stamps, B. Hillebrands, G. Guntherodt, Magnetic anisotropies of ultrathin Co(001) films on Cu(001), Phys. Rev. Lett. 69 (1992) 3674–3677.
[40] O. Heckmann, H. Magnan, P. Le Fevre, D. Chandesris, J.J. Rehr, Crystallographic structure of cobalt films on Cu (001): elastic deformation to a tetragonal structure, Surf. Sci. 312 (1994) 62–72.
[41] U. Ramsperger, A. Vaterlaus, P. Pfaffli, U. Maier, D. Pescia, Growth of Co on a stepped and on a flat Cu(001) surface, Phys. Rev. B 53 (1996) 8001–8006.
[42] Z.W. Fan, P. Li, E.Y. Jiang, H.L. Bai, High spin polarization induced by the interface hybridization in Co/C composite films, Carbon 50 (2012) 4470–4475.
[43] H. Wang, S.P. Wong, W.Y. Cheung, N. Ke, G.H. Wen, X.X. Zhang, R.W.M. Kwok, Magnetic properties and structure evolution of amorphous Co–C nanocomposite films prepared by pulsed filtered vacuum arc deposition, J. Appl. Phys. 88 (2000) 4919–4921.
[44] F. Djeghloul, M. Gruber, E. Urbain, D. Xenioti, L. Joly, S. Boukari, J. Arabski, H. Bulou, F. Scheurer, F. Bertran, P. Le Fevre, A. Taleb-Ibrahimi, W. Wulfhekel, G. Garreau, S. Hajjar-Garreau, P. Wetzel, M. Alouani, E. Beaurepaire, M. Bowen, W. Weber, High spin polarization at ferromagnetic metal-organic interfaces: a generic property, J. Phys. Chem. Lett. 7 (2016) 2310–2315.
[45] G.W. Ji, G.H. Zheng, B. Zhao, F. Song, X.N. Zhang, K.C. Shen, Y.G. Yang, Y. M. Xiong, X.Y. Gao, L. Cao, Interfacial electronic structures revealed at the rubrene/CH 3 NH 3 PbI 3 interface, Phys. Chem. Chem. Phys. 19 (2017) 6546–6553.
[46] S. Sinha, C.H. Wang, M. Mukherjee, Energy level alignment and molecular conformation at rubrene/Ag interfaces: impact of contact contaminations on the interfaces, Appl. Surf. Sci. 409 (2017) 22–28.
[47] Y.J. Hou, C.K. Yang, C.Y. Hsu, Y.W. Jhou, J.S. Tsay, Structural determination and magnetic properties for Co–rubrene composite films on Si (1 0 0), Appl. Phys. Lett. 354 (2015) 139–143.
[48] K.V. Raman, S.M. Watson, J.H. Shim, J.A. Borchers, J. Chang, J.S. Moodera, Effect of molecular ordering on spin and charge injection in rubrene, Phys. Rev. B 80 (2009), 195212.
[49] M.L. Zhu, L. Lyu, D.M. Niu, H. Zhang, S.T. Wang, Y.L. Gao, Effect of a MoO 3 buffer layer between C8-BTBT and Co (100) single-crystal film, RSC Adv. 6 (2016) 112403–112408.
[50] M.L. Zhu, L. Lyu, D.M. Niu, H. Zhang, Y.H. Zhang, P. Liu, Y.L. Gao, Interfacial chemical and electronic structure of cobalt deposition on 2,7-dioctyl[1]benzothieno [3,2-b]benzothiophene (C8-BTBT), Appl. Surf. Sci. 402 (2017) 142–146.
[51] L. Berbil-Bautista, S. Krause, T. Hänke, M. Bode, R. Wiesendanger, Spin-polarized scanning tunneling microscopy through an adsorbate layer: sulfur-covered Fe/W (110), Surf. Sci. 600 (2006) L20–L24.